Recursive Bayesian synthetic aperture geoacoustic inversion in the presence of motion dynamics

Bien Aik Tan,[a] Peter Gerstoft, Caglar Yardim, and William S. Hodgkiss
Marine Physical Laboratory, Scripps Institution of Oceanography, University of California San Diego, 9500 Gilman Drive, La Jolla, California 92093-0238

(Received 8 March 2014; revised 11 July 2014; accepted 30 July 2014)

A low signal to noise ratio (SNR), single source/receiver, broadband, frequency-coherent matched-field inversion procedure recently has been proposed. It exploits coherently repeated transmissions to improve estimation of the geoacoustic parameters. The long observation time improves the SNR and creates a synthetic aperture due to relative source-receiver motion. To model constant velocity source/receiver horizontal motion, waveguide Doppler theory for normal modes is necessary. However, the inversion performance degrades when source/receiver acceleration exists. Furthermore processing a train of pulses all at once does not take advantage of the natural incremental acquisition of data along with the ability to assess the temporal evolution of parameter uncertainty. Here a recursive Bayesian estimation approach is developed that coherently processes the data pulse by pulse and incrementally updates estimates of parameter uncertainty. It also approximates source/receiver acceleration by assuming piecewise constant but linearly changing source/receiver velocities. When the source/receiver acceleration exists, it is shown that modeling acceleration can reduce further the parameter estimation biases and uncertainties. The method is demonstrated in simulation and in the analysis of low SNR, 100–900 Hz linear frequency modulated (LFM) pulses from the Shallow Water 2006 experiment.
 [http://dx.doi.org/10.1121/1.4892788]

PACS number(s): 43.60.Pt [ZHM] Pages: 1187–1198

I. INTRODUCTION

Based on the signal measured at a receiver that is some distance away from the source, the general idea of geoacoustic inversion is to optimize the waveguide geoacoustic model parameters by minimizing the difference between the measured and the replica (modeled) acoustic fields. In doing this, seafloor properties are estimated without resorting to costly direct measurements such as coring. Knowing the seafloor acoustic properties is important for various applications such as sonar performance prediction.

Recently, a single-source/receiver, broadband, frequency coherent matched-field inversion procedure was proposed in Ref. 1. It exploits coherently repeated transmissions to improve estimation of the geoacoustic parameters in low signal to noise (SNR) conditions. The long observation time improves the SNR and creates a synthetic aperture due to relative source-receiver horizontal motion. However, due to the temporal extent of the data observation, source/receiver motion has to be taken in account using waveguide Doppler theory where each horizontal wavenumber or mode undergoes a different Doppler shift.[1–3] Though successful, the approach is limited to constant source/receiver radial velocities. Therefore the assumptions are violated in the region near the closest point of approach (CPA) or when the radial velocities change. This paper improves the broadband synthetic aperture geoacoustic inversion approach for cases where the radial velocity of the source/receiver changes. This is done through pulse-by-pulse coherent processing that in turn allows different source/receiver velocities.

Furthermore processing a train of pulses all at once does not take advantage of the natural incremental acquisition of new data along with the ability to assess the temporal evolution of parameter uncertainty. Here an equivalent pulse-by-pulse coherent processing approach using Bayesian updating is developed. With the Bayesian formulation, the estimated posterior distribution provides quantitative uncertainty analysis.[4] It also may be used to infer uncertainties in another usage domain (e.g., transmission loss[5]). This recursive Bayesian approach allows new data to be added incrementally without having to wait for all data to be present before processing can take place.[6] At present, most single source and receiver methods,[1,7–18] except Ref. 19, do not use the Bayesian approach for uncertainty analysis.

The improved method is well suited for rapid environment assessment using a moving source and/or receiver as depicted in Fig. 1. The source or receiver may be towed horizontally by a ship or an autonomous underwater vehicle (AUV). Alternatively, a battery powered acoustic source may be dropped onto the ocean bottom to aid AUV-based geoacoustic inversion.[20] AUV-based inversions recently have been gaining research interest due to their operational attractiveness.[21–24]

The theory of waveguide Doppler and modal propagation is reviewed briefly in Sec. II, followed by the formulation of the inversion problem. Simulation results are presented in Sec. III. Section IV presents results from the analysis of low SNR, 100–900 Hz LFM data from the Shallow Water 2006 experiment.

[a]Author to whom correspondence should be addressed. Electronic mail: btan@ucsd.edu

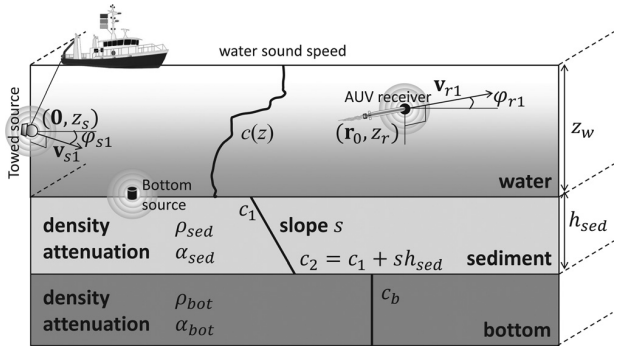

FIG. 1. Horizontally stratified ocean with a horizontally moving source and receiver. The source is moving at initial velocity $\mathbf{v}_{s1}$ and bearing φ_{s1}, while the receiver is moving at initial velocity $\mathbf{v}_{r1}$ and bearing φ_{r1}. The range origin is the source position at time zero when the source begins transmitting.

II. THEORY

An overview of the recursive Bayesian approach is illustrated in Fig. 2. At the lth measurement $\mathbf{y}_l$, the likelihood $p(\mathbf{y}_l|\mathbf{m})$ of the lth measurement conditioned on any particular set of model parameters $\mathbf{m}$ is computed (Sec. II B). This means computing the difference between the measured field $\mathbf{y}_l$ and the replica (modeled) field. Taking into the account of source/receiver motion, the replica field is generated using the waveguide Doppler model in Sec. II A.

The recursive Bayesian estimation approach is derived in Sec. II C. The general idea is to propagate the past posterior probability density $p(\mathbf{m}|\mathbf{y}_{1:l-1})$ as the prior information to improve the current posterior probability density $p(\mathbf{m}|\mathbf{y}_{1:l})$ with the current likelihood $p(\mathbf{y}_l|\mathbf{m})$ via Bayes' rule. The posterior density is represented with a set of samples of $\mathbf{m}$ and weights that are updated recursively as new measurements become available. However, as the posterior density evolves with the measurements, the importance density sampling the posterior density needs to adapt correspondingly where samples are added to the high probability regions of the posterior density. Sections II D and II E address the implementation of the recursive Bayesian estimation approach using adaptive importance sampling (AIS) of the time-evolving posterior density.

The assumptions for the forward model and inversion approach are listed in Table I.

A. Waveguide Doppler theory model for acceleration dynamics

In a waveguide, the impact of Doppler is complicated due to multipath. Discussions of waveguide Doppler include Refs. 2, 3, and 25–28. In this paper, waveguide Doppler due to source/receiver motion on a signal propagating in a range-independent waveguide is adapted from Schmidt and Kuperman.[2,3] Each horizontal wavenumber or mode undergoes a different Doppler shift. The scenario considered is depicted in Fig. 1. Based on constant source and receiver velocities and depth constraints, and a positive-exponent Fourier transform convention, the waveguide Doppler shifted field via a normal mode representation is[1]

TABLE I. Assumptions for the forward model and inversion approach.

Waveguide Doppler model (see Ref. 1 and Sec. II A)
• Range independent environment
• Known source spectrum
• $v/c \ll 1$, source/receiver speed v is much less than the acoustic wave propagation speed c
• $\mathbf{v}_{sl}$ and $\mathbf{v}_{rl}$ are constant and horizontal
• Source-receiver displacement (due to motion) is much less than the source-receiver separation. Therefore the radial velocities are approximately constant $v_{rl} = \lvert\mathbf{v}_{rl}\rvert \cos\varphi_{rl}$, $v_{sl} = \lvert\mathbf{v}_{sl}\rvert \cos\varphi_{sl}$
• $\Psi(z;\omega) \approx \Psi(z;\omega_r) \approx \Psi(z;\omega_s)$
• Cutoffs or additions of modes due to Doppler shifts are neglected
• $k_{nl} \approx k_{rn}/[1-(v_{rl}/u_{rn})] \approx k_{sn}/[1-(v_{sl}/u_{sn})]$ where k_{nl} is approximated through Taylor's first order expansion
• Source/receiver acceleration is constant and much smaller than source/receiver speed
Recursive Bayesian inversion (see Secs. II B and II C)
• Initial prior knowledge of the parameters
• Underlying model parameters are constant for all measurements

$$\psi(\mathbf{r}, z_r, \omega_r) \approx \frac{ie^{-i(\pi/4)}}{\sqrt{8\pi}\rho(z_s)} \sum_n S\left[\omega_s^{(k_n)}\right] \times \Psi_n(z_r;\omega_r)\Psi_n(z_s;\omega_r)\frac{e^{ik_n r_0}}{\sqrt{k_n r_0}}, \quad (1)$$

where

$$\omega_s^{(k_n)} = \omega_r - k_n(v_s - v_r), \quad (2)$$

$$k_n \approx \frac{k_{rn}}{\left(1 - \frac{v_r}{u_{rn}}\right)}, \quad (3)$$

$$S(\omega_s) = \sum_{l=1}^{L} \exp[i\omega_s(l-1)T_r]S_c(\omega_s). \quad (4)$$

r_0 is the source-receiver separation at $t = 0$. v_s, v_r, z_s, and z_r are the radial source and receiver velocities and depths, respectively. $\rho(z_s)$ is the water density. k_n and Ψ_n are the modal wavenumbers and modal functions evaluated at propagation frequencies ω. For numerical efficiency, constructing the field in Eq. (1) is facilitated by some approximations to the propagation modal wavenumbers and functions that

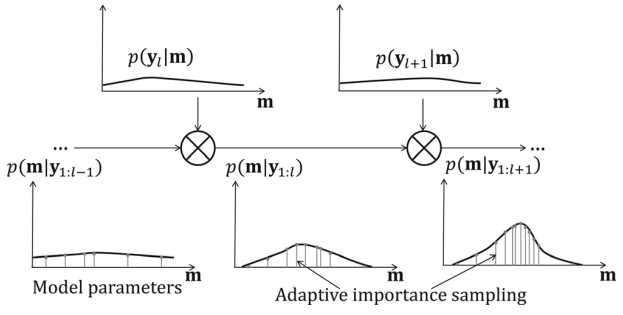

FIG. 2. Recursive Bayesian approach. The lth measurement is $\mathbf{y}_l$, and $\mathbf{m}$ is the vector of model parameters. For illustration purpose, $\mathbf{m}$ is depicted here as a scalar. The posterior density $p(\mathbf{m}|\mathbf{y}_{1:l})$ is represented with a set of samples of $\mathbf{m}$ and weights. The importance density changes by introducing new samples from other densities as the posterior density evolves.

are computed instead at the receiver frequency ω_r [see Eqs. (1) and (3)]. $\omega_s^{(k_n)}$ is the mode-dependent source frequency mapping function used to construct the field at ω_r. $u_{rn} = d\omega_r/dk_n(\omega_r)$ is the nth modal group velocity and $k_{rn} = k_n(\omega_r)$ is the nth modal wavenumber, both evaluated at ω_r. $S(\omega_s)$ is the source spectrum of L pulses representing the amplitude and phase of the moving point source. T_r is the pulse repetition interval (PRI) and $S_c(\omega_s)$ is the spectrum of the common or repeated source transmission.

When the source traverses past the receiver, the radial velocity v_s changes even though the source velocity $\mathbf{v_s}$ is constant (see Fig. 3). As shown later in Sec. III, acceleration needs to be modeled to perform a meaningful inversion near the CPA. However, modeling acceleration is non-trivial as it results in time-dependence in the modal wavenumbers and modal functions.[29] As an approximation to a constant acceleration, a practical approach is to assume multiple short duration transmissions, e.g., multiple pulses as in Eq. (4), where the source/receiver radial velocities are assumed piecewise constant for the lth pulse but linearly changing from pulse to pulse. Therefore the field can be generated for each pulse and coherently combined for L pulses to form the received spectrum. Substituting Eqs. (4) and (2) into Eq. (1) and introducing pulse number dependent radial velocities, the replica field may be represented as a sum of L fields $\psi_l(\mathbf{r}, z_r, \omega_r)$ such that

$$\psi(\mathbf{r}, z_r, \omega_r) = \sum_{l=1}^{L} \psi_l(\mathbf{r}, z_r, \omega_r), \tag{5}$$

where

$$\psi_l(\mathbf{r}, z_r, \omega_r) = \frac{ie^{-i(\pi/4)}}{\sqrt{8\pi}\rho(z_s)} \exp[i\omega_r(l-1)T_r] \times \sum_n S_c\left[\omega_s^{(k_n,l)}\right] \Psi_n(z_r; \omega_r) \times \Psi_n(z_s; \omega_r) \frac{e^{ik_{nl}r_{0l}}}{\sqrt{k_{nl}r_{0l}}}, \tag{6}$$

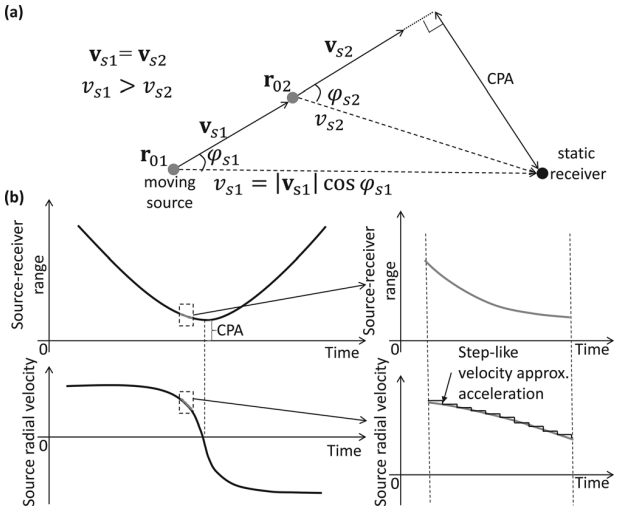

FIG. 3. (a) Top view of a constant velocity source with changing radial velocity to the receiver due to the geometry of source/receiver positions. (b) Source–receiver range and radial velocity curves near CPA. Here the change in source radial velocity in the dotted box approximately is linear with time corresponding to a constant acceleration.

$$\omega_s^{(k_{nl})} = \omega_r - k_{nl}(v_{sl} - v_{rl}), \tag{7}$$

$$k_{nl} \approx \frac{k_{rn}}{\left(1 - \frac{v_{rl}}{u_{rn}}\right)}, \tag{8}$$

$$v_{sl} = v_{s1} + (l-1)T_r a_s, \tag{9}$$

$$v_{rl} = v_{r1} + (l-1)T_r a_r, \tag{10}$$

and

$$r_{0l} = \begin{cases} r_0, & \text{if } l = 1, \\ r_0 + \sum_{j=1}^{l-1} T_r(v_{rj} - v_{sj}), & \text{if } l = 2, \ldots, L. \end{cases} \tag{11}$$

Each pulse is propagated in the forward model with its corresponding values of v_{sl} and v_{rl} then coherently combined in Eq. (5). Note that all L pressure fields still are referenced to $t = 0$. In Eq. (8), the horizontal wavenumber k_{nl} depends on mode n and pulse number l. Hence there also are mode and pulse number dependent frequency mappings when tracing back to ω_s in order to construct the field at ω_r, see Eq. (7). As an approximation to a constant acceleration, the source/receiver radial velocities v_{sl} and v_{rl} [Eqs. (9) and (10)] are modeled to be piecewise constant for the lth pulse but linearly changing from pulse to pulse. a_s and a_r are the source and receiver radial accelerations, respectively.

B. Likelihood functions

The broadband data model for frequency-coherent match-field based geoacoustic inversion can be expressed as L measurement vectors,

$$\mathbf{y}_l = \alpha \mathbf{E}(\xi)\mathbf{d}_l(\mathbf{m}) + \mathbf{g}_l = \alpha \mathbf{b}_l(\xi, \mathbf{m}) + \mathbf{g}_l, \tag{12}$$

where $\mathbf{y}_l = [y_l(\omega_{r1}) \cdots y_l(\omega_{rJ})]^{\mathrm{T}}$ is the K-point fast Fourier transform (FFT) of the observed time series capturing the lth pulse for J discrete frequencies. Note the lth pulse Fourier transforms are synchronized to the first pulse transmission time ($t = 0$) so that only one timing error ξ between the source and receiver clocks needs to be resolved. $\mathbf{E}(\xi)$ is a diagonal matrix for correcting the timing error, $\mathbf{E}(\xi) = \mathrm{diag}[e^{i\omega_{r1}\xi} \cdots e^{i\omega_{rJ}\xi}]$. $\mathbf{m}$ is the subset of forward model parameters that are being estimated (see Fig. 1). α is a scale factor representing the unknown source level. To introduce source/receiver motion or waveguide Doppler, the corresponding replica field $\mathbf{d}_l(\mathbf{m}) = [\psi_l(\omega_{r1}, \mathbf{m}) \cdots \psi_l(\omega_{rJ}, \mathbf{m})]^{\mathrm{T}}$ is generated using Eq. (6) with vector $\mathbf{m}$. It is assumed the model parameters $\mathbf{m}$, α and ξ do not change between measurements and thus the joint likelihood function will sharpen as L increases.

The distribution of the error vector $\mathbf{g}_l = [g_l(\omega_{r1}) \cdots g_l(\omega_{rJ})]^{\mathrm{T}}$ defines the likelihood function. It is assumed that $\mathbf{g}_l$ for $l = 1, \ldots, L$ are independent and identically distributed (i.i.d.) across L measurements. Error consists of both ambient noise and modeling errors. For low SNR processing, the colored ambient noise will be considered the dominant

source of error. The frequency-dependent noise is modeled as a wide sense stationary noise $u[n]$ with power spectral density $P_{uu}(\omega_r)$. $P_{uu}(\omega_r)$ is estimated from noise only data prior to the pulse transmissions.

Taking a K-point FFT of $u[n]$, let the lth error vector $\mathbf{g}_l$ be the FFT of $u[n]$ evaluated at frequencies $[\omega_{r1} \cdots \omega_{rJ}]$ with $J \leq K$. We will define the frequency domain noise $\mathbf{g}_l$ as complex Gaussian with mean $\mathrm{E}[\mathbf{g}_l] = \mathbf{0}$ for $\omega_r \neq 0$ and autocovariance[30]

$$\mathbf{C}_\mathbf{g} = \mathrm{E}[\mathbf{g}_l \mathbf{g}_l^{\mathrm{H}}] = \gamma \mathrm{diag}[P_{uu}(\omega_{r1}) \cdots P_{uu}(\omega_{rJ})], \tag{13}$$

where γ is a scale factor for scaling the noise spectrum in the data inversions. Thus it is assumed that the error vector $\mathbf{g}_l \sim \mathcal{CN}(\mathbf{0}, \mathbf{C}_\mathbf{g})$. Factoring $\mathbf{C}_\mathbf{g} = \gamma \tilde{\mathbf{C}}_\mathbf{g}$ with $\tilde{\mathbf{C}}_\mathbf{g} = \mathrm{diag}[P_{uu}(\omega_{r1}) \cdots P_{uu}(\omega_{rJ})]$, the joint likelihood function of the L measurements can be expressed as (based on i.i.d. measurements)

$$\begin{aligned}\mathcal{L}(\tilde{\mathbf{m}}) = p(\mathbf{y}_{1:L}|\tilde{\mathbf{m}}) = \prod_{l=1}^{L} p(\mathbf{y}_l|\tilde{\mathbf{m}}) = \prod_{l=1}^{L} \frac{1}{(\pi\gamma)^J |\tilde{\mathbf{C}}_\mathbf{g}|} \\ \times \exp\{-[\mathbf{y}_l - \alpha \mathbf{b}_l(\xi, \mathbf{m})]^{\mathrm{H}} \tilde{\mathbf{C}}_\mathbf{g}^{-1} \\ \times [\mathbf{y}_l - \alpha \mathbf{b}_l(\xi, \mathbf{m})]/\gamma\},\end{aligned} \tag{14}$$

where supervector $\mathbf{y}_{1:L} = [\mathbf{y}_1^{\mathrm{T}}, \ldots, \mathbf{y}_L^{\mathrm{T}}]^{\mathrm{T}}$ and $\tilde{\mathbf{m}} = [\mathbf{m}^{\mathrm{T}}, \gamma, \alpha, \xi]^{\mathrm{T}}$. To simplify the notation, $\mathbf{m}$ is now redefined to also include γ, α, and ξ. For this empirical Bayesian estimation problem, α and γ are estimated jointly with the model parameters,[5] instead of incorporating their maximum likelihood estimates (MLE) as in Ref. 1.

C. Recursive Bayesian estimation

In low SNR conditions, long time integration is necessary for acceptable parameter estimation uncertainty. The time-dependent source-receiver range can be recast into a set of initial value and constant parameters. This reformulation includes initial value parameter such as initial source range r_0 at $(t = 0)$ [Eq. (11)], initial velocities v_{s1} and v_{r1} and constant accelerations a_s and a_r [Eqs. (9) and (10)] for use with the waveguide Doppler model [Eqs. (5) and (6)]. Thus the need to track[31,32] the time-dependent source-receiver range is circumvented, and the measurements accumulate and improve the likelihood/posterior densities. It is assumed that other model parameters, such as the seafloor properties, do not change for the L measurements.

Recursive Bayesian estimation (see Fig. 2) is inspired by recursive Bayesian online learning and particle filter theories.[6,33–36] With initial prior knowledge of the parameters $p(\mathbf{m})$ and Bayes' rule, the joint posterior probability density function (PPD) of the model parameters for l pulse measurements is[6]

$$p(\mathbf{m}|\mathbf{y}_{1:l}) = \frac{p(\mathbf{y}_{1:l}|\mathbf{m})p(\mathbf{m})}{p(\mathbf{y}_{1:l})} \tag{15}$$

$$= \frac{p(\mathbf{y}_l|\mathbf{m})p(\mathbf{m}|\mathbf{y}_{1:(l-1)})}{\int p(\mathbf{y}_l|\mathbf{m})p(\mathbf{m}|\mathbf{y}_{1:(l-1)})\mathrm{d}\mathbf{m}}. \tag{16}$$

Equation (16) shows that the joint posterior density conditioned on l measurements can be updated recursively from the lth likelihood and the joint posterior density of the $l-1$ measurements. Thus Bayesian updating of $p(\mathbf{m}|\mathbf{y}_{1:l})$ can be done all at once [Eq. (15)] or recursively over time [Eq. (16)]. In addition, assuming constant geoacoustic model parameters for all l, no model mismatch error and no bias error between the replica and measured fields, the variance of the maximum *a posteriori* (MAP) parameter estimate,

$$\mathrm{var}[\hat{\mathbf{m}}_{MAP}^{(L)}] < \mathrm{var}[\hat{\mathbf{m}}_{MAP}^{(L-1)}] < \cdots < \mathrm{var}[\hat{\mathbf{m}}_{MAP}^{(1)}], \tag{17}$$

where

$$\hat{\mathbf{m}}_{MAP}^{(L)} = \arg\max_{\mathbf{m}} p(\mathbf{m}|\mathbf{y}_{1:L}) = \arg\max_{\mathbf{m}} p(\mathbf{m}) \prod_{l=1}^{L} p(\mathbf{y}_l|\mathbf{m}). \tag{18}$$

Ideally, the posterior density converges to a Dirac delta function centered at the true parameter value as L approaches infinity.[6] Practically, it is difficult to attain the true parameter value as there will be some model mismatch error or bias in the estimator. In addition, only a limited number of measurements can be processed before time-dependent variations in the model parameters and model mismatch errors become significant.

D. Recursive Monte Carlo integration and importance sampling

The posterior density $p(\mathbf{m}|\mathbf{y}_{1:l})$ is used to compute metrics of interest such as the MAP estimates, posterior means, variances and marginal PPDs of the model parameter m_i (Refs. 4 and 37) [see Eqs. (18) and (19)–(22)]. A way of generating these metrics is Monte Carlo integration and importance sampling.[38–41] Compared to Markov Chain Monte Carlo methods that sequentially sample the posterior density, the primary appeal of importance sampling is the ability to carry out large-scale sampling of the posterior density in parallel. These metrics also can be updated as new data is made available [see Eqs. (27)–(29)],

$$\mu_i = \int m_i p(\mathbf{m}|\mathbf{y}_{1:l})\,\mathrm{d}\mathbf{m}, \tag{19}$$

$$\sigma_i^2 = \int (m_i - \mu_i)^2 p(\mathbf{m}|\mathbf{y}_{1:l})\,\mathrm{d}\mathbf{m}, \tag{20}$$

$$p(m_i|\mathbf{y}_{1:l}) = \int \delta(m'_i - m_i) p(\mathbf{m}'|\mathbf{y}_{1:l})\,\mathrm{d}\mathbf{m}', \tag{21}$$

$$\begin{aligned}p(m_i, m_j|\mathbf{y}_{1:l}) = \int \delta(m'_i - m_i)\delta(m'_j - m_j) \\ \times p(\mathbf{m}'|\mathbf{y}_{1:l})\,\mathrm{d}\mathbf{m}'.\end{aligned} \tag{22}$$

For a parameter of interest such as the water column sound speed profile (SSP), c_w, that is inferred from the inversion and is a function of empirical orthogonal functions (EOFs)

and coefficients,[1,42–44] $c_w = C(\mathbf{m})$, the probability distribution of c_w is[4,5]

$$p(c_w|\mathbf{y}_{1:l}) = \int \delta[c_w - C(\mathbf{m})] p(\mathbf{m}|\mathbf{y}_{1:l})\, d\mathbf{m}. \tag{23}$$

As shown later in Sec. IV A, Eq. (23) is used to plot the SSP estimation uncertainty in Figs. 12–14. Using the Monte Carlo integration method,[38–41] these integrals are of the form,

$$\int h(\mathbf{m}) p(\mathbf{m}|\mathbf{y}_{1:l})\, d\mathbf{m} = \mathrm{E}[h(\mathbf{m})] \approx \frac{1}{Q}\sum_{q=1}^{Q} h(\mathbf{m}^q), \tag{24}$$

where the samples $\{\mathbf{m}^q, q = 1, \ldots, Q\}$ are drawn from the distribution $p(\mathbf{m}|\mathbf{y}_{1:l})$. Drawing samples from $p(\mathbf{m}|\mathbf{y}_{1:l})$ is difficult as it usually is a non-standard and high dimensional probability density function (PDF).[39,40] Alternatively, a standard or importance density $x(\mathbf{m})$ may be used to generate the samples. This is known as importance sampling.[38–40] Therefore

$$\int h(\mathbf{m}) p(\mathbf{m}|\mathbf{y}_{1:l})\, d\mathbf{m} \approx \frac{\sum_{q=1}^{Q} h(\mathbf{m}^q)\tilde{w}_l^q}{\sum_{j=1}^{Q} \tilde{w}_l^j}, \tag{25}$$

where

$$\tilde{w}_l^q = \frac{p(\mathbf{y}_{1:l}|\mathbf{m}^q)p(\mathbf{m}^q)}{x(\mathbf{m}^q)} \tag{26}$$

are the unnormalized weights, and they correct under- and over-represented samples drawn from $x(\mathbf{m})$ instead of $p(\mathbf{m}|\mathbf{y}_{1:l})$. However, Eqs. (25) and (26) are non-recursive. As new data is made available, the weights may be computed recursively as[33–35]

$$\tilde{w}_l^q = p(\mathbf{y}_l|\mathbf{m}^q)\tilde{w}_{l-1}^q. \tag{27}$$

Let normalized weights be $w_l^q = \tilde{w}_l^q / \sum_{j=1}^{j=Q} \tilde{w}_l^j$. Equation (25) becomes

$$\int h(\mathbf{m}) p(\mathbf{m}|\mathbf{y}_{1:l})\, d\mathbf{m} \approx \sum_{q=1}^{Q} h(\mathbf{m}^q) w_l^q. \tag{28}$$

Equations (27) and (28) are recognized as an implementation of Eq. (16). The PPD can be approximated by[33,34]

$$p(\mathbf{m}|\mathbf{y}_{1:l}) \approx \sum_{q=1}^{Q} \delta(\mathbf{m} - \mathbf{m}^q) w_l^q, \tag{29}$$

and it approaches the true PPD as $Q \to \infty$. For comparison, see Eqs. (21) and (22).

E. Adaptive importance sampling

The PPDs, $p(\mathbf{m}|\mathbf{y}_{1:l})$, evolve with each new pulse. Thus the importance density is a function of l and should adapt correspondingly to sample the evolving PPDs effectively. One solution is to employ a Gaussian mixture for the importance density. Let the importance density be given by[45,46]

$$x(\mathbf{m};\, l) = \sum_{n=0}^{l} \beta_n x_n(\mathbf{m}), \tag{30}$$

where the mixture coefficients $\beta_n = Q_n/Q$, Q_n is the number of samples generated from the nth Gaussian density $x_n(\mathbf{m})$ and $Q = \sum_{n=0}^{l} Q_n$, and thus $\sum_{n=0}^{l} \beta_n = 1$.

Conventionally, Gaussian mixtures are used in adaptive importance sampling (AIS) to match the arbitrary and non-evolving PPD (in Bayesian applications).[45,46] The mixture coefficients, means and covariance matrices of $x_n(\mathbf{m})$ are adaptively improved based on the previous Monte Carlo draws that sample the same PPD. In addition, the number of densities in the mixture remains constant. However, adapting the mixture coefficients β_n, means and variances of $x_n(\mathbf{m})$ is computationally demanding for each pulse measurement in the application discussed here. This is because each adaptive iteration requires hundreds or more forward model evaluations, and many iterations are needed for the AIS density to converge to the current posterior density.

A simple alternative use of the Gaussian mixture that directly uses the posterior information is proposed here. The main difference between previous AIS implementations[45,46] and our proposed AIS is that the importance density here (Figs. 4 and 7) iteratively adapts as the PPD $p(\mathbf{m}|\mathbf{y}_{1:l})$ changes with l. The pseudo code for recursive Bayesian estimation using AIS is provided in Table II. There are $l+1$ mixture components for a PPD conditioned on l measurements (see Eq. 30 and Fig. 4).

The initial density $x_0(\mathbf{m})$ is used in a preliminary exploration of $p(\mathbf{m}|\mathbf{y}_1)$. $x_0(\mathbf{m})$ is chosen to be a Gaussian density $\mathcal{N}((\mathbf{s}_u + \mathbf{s}_l)/2, \mathrm{diag}[(\mathbf{s}_u - \mathbf{s}_l)/2]^2)$, where $\mathbf{s}_u$ and $\mathbf{s}_l$ are upper and lower boundaries of the parameter search space. Using importance samples drawn from $x_0(\mathbf{m})$ and the first pulse measurement, $\hat{\mathbf{m}}_{MAP}^{(1)}$ and the covariance matrix $\mathbf{C}_1$ of $\mathbf{m}$ can be approximated [see Eqs. (18), (19), and (31)]. While retaining the old importance samples for a new pulse, an additional set of importance samples is included using the density $x_1(\mathbf{m}) = \mathcal{N}(\hat{\mathbf{m}}_{MAP}^{(1)}, \mathbf{C}_1)$. Then, using $\sum_{j=0}^{1} Q_j$ importance samples from $x_0(\mathbf{m})$ and $x_1(\mathbf{m})$, $\hat{\mathbf{m}}_{MAP}^{(l)}$, and $\mathbf{C}_1$ can be updated.

It is important to note that both $\hat{\mathbf{m}}_{MAP}^{(l)}$ and $\mathbf{C}_l$ first are approximated from the PPD $p(\mathbf{m}|\mathbf{y}_{1:l})$ using the previous $\sum_{j=0}^{l-1} Q_j$ importance samples and the current pulse measurement embedded in the updated weights w_l^q. Subsequently, importance samples are drawn from $\mathcal{N}(\hat{\mathbf{m}}_{MAP}^{(l)}, \mathbf{C}_l)$ to sample the PPD $p(\mathbf{m}|\mathbf{y}_{1:l})$ more effectively. Then, using past and present importance samples $\sum_{j=0}^{l} Q_j$, $\hat{\mathbf{m}}_{MAP}^{(l)}$ and $\mathbf{C}_l$ can be updated. $\mathbf{C}_l$ is computed from [see Eqs. (18) and (19)][39,41]

$$\mathbf{C}_l \approx \sum_{q=1}^{Q} (\mathbf{m}^q)(\mathbf{m}^q)^{\mathrm{T}} w_l^q - \boldsymbol{\mu}_l \boldsymbol{\mu}_l^{\mathrm{T}}. \tag{31}$$

The importance density $x(\mathbf{m};\, l)$ now is dependent on l. The weight corrections [Eq. (26)] should be applied after the weight recursion but before the weight normalization. Let un-corrected and un-normalized weights be redefined as $\hat{w}_l^q = p(\mathbf{y}_{1:l}|\mathbf{m}^q)p(\mathbf{m}^q)$ and the new recursion be $\hat{w}_l^q = p(\mathbf{y}_l|\mathbf{m}^q)\hat{w}_{l-1}^q$. The weights then are corrected by $\tilde{w}_l^q = \hat{w}_l^q / x(\mathbf{m}^q;\, l)$ before normalization. Importance sampling

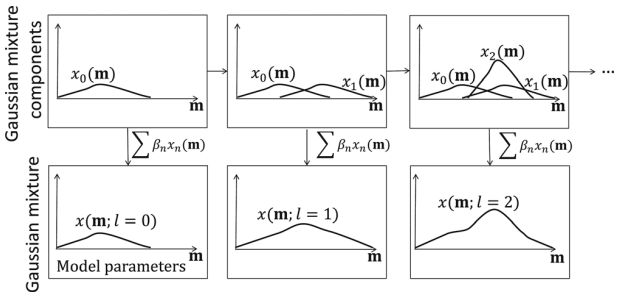

FIG. 4. Importance density evolution with l.

potentially can have numerical stability issues in the weight correction $\tilde{w}_l^q = \hat{w}_l^q / x(\mathbf{m}^q; l)$ if $x(\mathbf{m}^q; l)$ is very small. Retaining the older densities in the mixture has the desirable effect of increasing the tails of the overall density while maintaining the main mass of samples in the high PPD region.[39,40]

The overall effect of this cumulative update of $\hat{\mathbf{m}}_{MAP}^{(l)}$ and $\mathbf{C}_l$ and accumulation of Gaussian densities is an AIS process. The last Gaussian density added will have a covariance that is an estimate of the covariance of the current PPD.

III. RECURSIVE BAYESIAN SIMULATION

This section will demonstrate the recursive Bayesian estimation approach that coherently processes the data pulse by pulse and incrementally updates estimates of parameter uncertainty. It also approximates source/receiver radial acceleration by assuming piecewise constant but linearly changing source/receiver velocities. When source/receiver radial acceleration exists, it is demonstrated that modeling acceleration [Eqs. (5)–(11)] can further reduce the parameter estimation biases and uncertainties. The ocean model is illustrated in Fig. 1 and model parameters are tabulated in Table III. Based on the theory presented in Sec. II A, this simulation models a constant velocity moving source that is slowing down radially with respect to the static receiver for $L = [1, \ldots, 64]$ pulses (see Fig. 3). The range-independent geoacoustic parameters were based on previous SW06 inversion results.[1,43,44,47,48] The source emits 100–900 Hz LFM pulses with 1 s pulse width and PRI. Thus $v_{s64} = 1.52$ m/s. [see Eq. (9)]. The noise, Eq. (13), was generated to be similar to the measured power spectrum of SW06 ambient noise data. The frequency sampling is 5 Hz starting from 100 to 700 Hz. KRAKEN is used to compute the modes and wavenumbers.[49]

The sediment parameters (ρ_{sed}, c_1, s, and α_{sed}) are estimated using the recursive Bayesian estimation procedure in Sec. II D, while the rest of the model parameters are assumed known. The parameter search space is kept small so that exhaustive-search based on 24^4 samples (instead of random importance samples) can be used to plot the true PPDs. Source acceleration is modeled in the replica field using Eq. (9). We first show that the method does indeed reduce the parameter uncertainty as L increases. Using Eqs. (21), (22), (27), and (28), Fig. 5 shows both one-dimensional (1-D) (along the diagonal) and two-dimensional (2-D) (off-diagonal) marginal PPDs. In the 2-D PPDs, the densities are contoured according to their percentage highest posterior density (HPD) regions.[4,37] This percentage HPD is also equal to percentage of the total probability. The PPDs of the model parameters are not Gaussian. This is due to the non-linear relationship between the acoustic field and the geoacoustic parameters. Comparing the posterior densities in Figs. 5(a) and 5(b), the reduction in the HPD regions indicates that there is much improvement. The 2-D PPDs also provide information about the correlation between any two parameters.

TABLE II. Pseudo code for recursive Bayesian estimation using adaptive importance sampling.

Preliminary exploration of PPD $p(\mathbf{m}|\mathbf{y}_1)$

Draw Q_0 samples $\{\mathbf{m}^1 \cdots \mathbf{m}^{Q_0}\}$ from density
$x_0(\mathbf{m}) \sim \mathcal{N}((\mathbf{s}_u + \mathbf{s}_l)/2, \text{diag}[(\mathbf{s}_u - \mathbf{s}_l)/2]^2)$
Initialize weights $\hat{w}_0^q = p(\mathbf{m}^q)$

Recursive Bayesian estimation
for $l = 1$ to L
  Using current lth measurement $\mathbf{y}_l$
  and the past importance samples $Q = \sum_{j=0}^{l-1} Q_j$:
    Update weights $\hat{w}_l^q = p(\mathbf{y}_l|\mathbf{m}^q)\hat{w}_{l-1}^q$
    Correct weights $\tilde{w}_l^q = \hat{w}_l^q / x(\mathbf{m}^q; l-1)$
    Normalize weights $w_l^q = \tilde{w}_l^q / \sum_{j=1}^{j=Q} \tilde{w}_l^j$
    Using the $(l-1)$ th importance density $x(\mathbf{m}; l-1)$
      Approximate MAP estimate $\hat{\mathbf{m}}_{MAP}^{(l)}$ Eq. (18)
      Approximate PPD covariance $\mathbf{C}_l$ Eqs. (19) and (31)
  Draw Q_l importance samples from density
  $x_l(\mathbf{m}) \sim \mathcal{N}(\hat{\mathbf{m}}_{MAP}^{(l)}, \mathbf{C}_l)$.
  For the new Q_l importance samples:
    Compute weights $\hat{w}_l^q = p(\mathbf{m}^q) \prod_{j=1}^{l} p(\mathbf{y}_j|\mathbf{m}^q)$
  For all importance samples $Q = \sum_{j=0}^{l} Q_j$:
    Correct weights $\tilde{w}_l^q = \hat{w}_l^q / x(\mathbf{m}^q; l)$
    Normalize weights $w_l^q = \tilde{w}_l^q / \sum_{j=1}^{j=Q} \tilde{w}_l^j$
  Bayesian statistical estimation for $\mathbf{y}_{1:l}$
    Finalize MAP estimate $\hat{\mathbf{m}}_{MAP}^{(l)}$ Eq. (18)
    Finalize covariance $\mathbf{C}_l$ Eqs. (19) and (31)
    Compute PPD estimate Eqs. (21), (22), and (29)
    Compute Bayesian inference Eqs. (23) and (29)
endfor

TABLE III. Baseline model parameters.

Simulation model parameters	Value
Source range at $t = 0$, r_0 (m)	600
Source depth, z_{s1} (m)	30
Receiver depth, z_{r1} (m)	45
Source initial radial velocity, v_{s1} (m/s)	1.9
Receiver initial radial velocity, v_{r1} (m/s)	0
Source radial acceleration, a_s (mm/s^2)	−6
Receiver radial acceleration, a_r (mm/s^2)	0
Water depth, z_w (m)	78
Sediment depth, h_{sed} (m)	22
Sediment density, ρ_{sed} (g/cm^3)	1.8
Sediment attenuation., α_{sed} (dB/λ)	0.2
Sediment top velocity, c_1 (m/s)	1640
Sediment velocity slope, s (1/s)	0
Bottom density, ρ_{bot} (g/cm^3)	2.2
Bottom attenuation., α_{bot} (dB/λ)	0.2
Bottom velocity, c_b (m/s)	1740

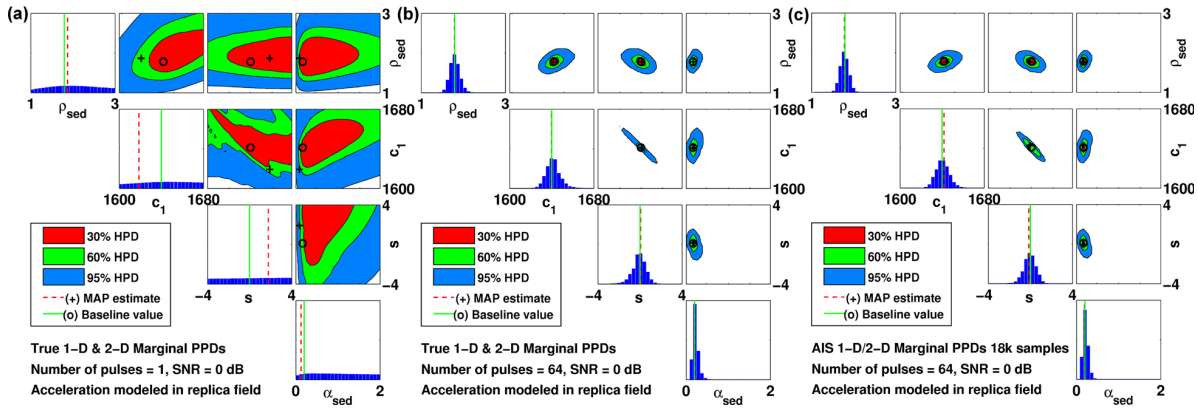

FIG. 5. (Color online) True marginal PPD via 24^4 exhaustive-search based samples with SNR fixed at 0 dB and number of LFM pulses (a) $L = 1$ (b) $L = 64$. (c) Estimated marginal PPD via AIS 18 120 samples with SNR fixed at 0 dB and number of LFM pulses $L = 64$.

Recursive Bayesian estimation is repeated with no source acceleration modeled [$a_s = 0$ in Eq. (9)] in the replica field while the measured field contains $a_s = -0.006$ m/s. As the number of pulse measurements increases, the replica-to-measured field mismatch increases and the MAP and PPD estimation results deteriorate and deviate from the baseline values [see Fig. 6(a)]. This is due to the replica field not modeling pulse-number (l) dependent radial velocity changes. In addition, the importance sampling utilized in this recursive Bayesian formulation also will have difficulty sampling the high probability regions of parameter space because there is a range of possible radial velocities to match. As a result, the MAP estimates and 1-D marginal PPD plots in Fig. 6(a) were adversely affected and provided little or biased information about the geoacoustic properties.

On the other hand, if source acceleration is modeled in the replica field, the joint PPD of the model parameters will evolve and be more informative (peaky) as the number of pulse measurements increases, Eq. (16). Equivalently, this is observed in Fig. 6(b) in the evolution of the 1-D marginal PPDs with increasing number of pulse measurements.

Figures 5(b) and 6(b) are repeated using the AIS approach starting with only 3000 samples that eventually grows to 18 120 samples [see Figs. 5(c) and 6(c)]. Comparing Figs. 5(b) and 5(c) and 6(b) and 6(c), the AIS PPDs look similar to the true PPDs, and they gradually will converge to the true PPD as more AIS samples are added. This has demonstrated that AIS is effective in estimating the PPD using 15 times less importance samples than the number used for the exhaustive sampling method. Figure 7 shows how the AIS importance distribution $x(\mathbf{m}; L)$ adaptively changes with L to follow the evolving PPD.

These simulations have demonstrated the reduction of biases and uncertainty of parameter estimates as L increases. There are two contributions to this improvement. One is the coherent gain from processing multiple pulses. The other is the spatial gain when the source moves toward the receiver. A way to check the incremental contribution due to spatial gain is to carry out a parameter sensitivity analysis comparing static and moving source–receiver configurations for 64 pulses (see Fig. 8). As the synthetic aperture created in this simulation is short (109 m), the synthetic aperture/spatial gain is not significant compared to the gain from processing multiple pulses.

IV. EXPERIMENTAL DATA ANALYSIS

The SW06 experiment was carried out near the shelf break on the New Jersey continental shelf from July to September 2006. The sequence of transmission in Ref. 1 do

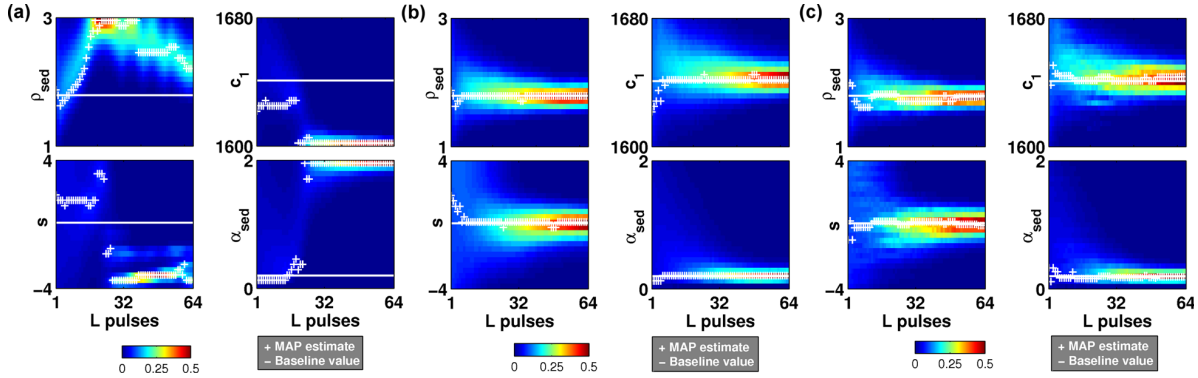

FIG. 6. (Color online) True 1-D marginal PPD evolution with $L = [1, \ldots, 64]$: (a) Acceleration not modeled in the replica field, (b) acceleration modeled in the replica field. (c) Estimated 1-D marginal PPD evolution with $L = [1, \ldots, 64]$ with acceleration modeled in the replica field and 3000–18 120 AIS samples.

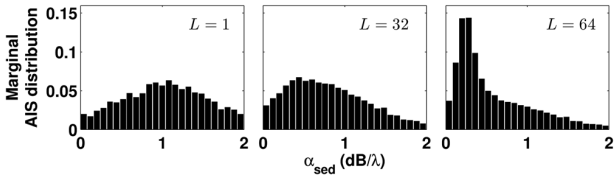

FIG. 7. AIS importance distribution $x(\mathbf{m}; L)$ marginalized onto α_{sed} for $L = [1, 32, 64]$.

not have enough acceleration to demonstrate the effects of modeling motion dynamics. Hence a new sequence that is closer to the CPA was selected for analysis. The data set has a linearly changing radial velocity moving source and a static receiver over a range-independent track, see Figs. 9 and 10. The acoustic data were recorded on JD238 2040 coordinated universal time (UTC) ($t = 0$) from a 44.6 m deep single receiver (Channel 8) of a vertical line array (VLA1). The data set consisted of 64 LFM pulse (100–900 Hz) transmissions from a 29.5 m deep J–15 source towed by the R/V Knorr at an initial radial velocity of 1.6 m/s and radial acceleration of -0.006 m/s^2. The LFM pulse width was 1 s and was repeated every second. The initial R/V Knorr global positioning system (GPS) range to VLA1 was 525 m with a CPA distance of 410 m and the source is known to be trailing 115 m behind the ship's GPS mast. Based on the ship and VLA1 positions, the actual source to VLA1 distance at $t = 0$ is estimated to be 603 m. In addition, by factoring in that the source is trailing 115 m behind the GPS antenna, the actual radial velocity between source and VLA1 is 1.9 m/s. Correspondingly, the towed source displacement with respect to VLA1 or synthetic aperture is $[1.9\,\text{m/s} - 64\,\text{s}/2 \times (0.006\,\text{m/s}^2)] \times 64\,\text{s} = 109\,\text{m}$ long.

The water depths measured at the source and receiver were 78 and 79 m, respectively. Water column SSPs are important and considered sensitive parameters in geoacoustic inversion. In the simulation, the SSP was assumed known to simplify and compute the true PPD. The true PPD confirms empirically that AIS in the inversion adequately samples the PPD (see Fig. 5). In the SW06 experimental data, the

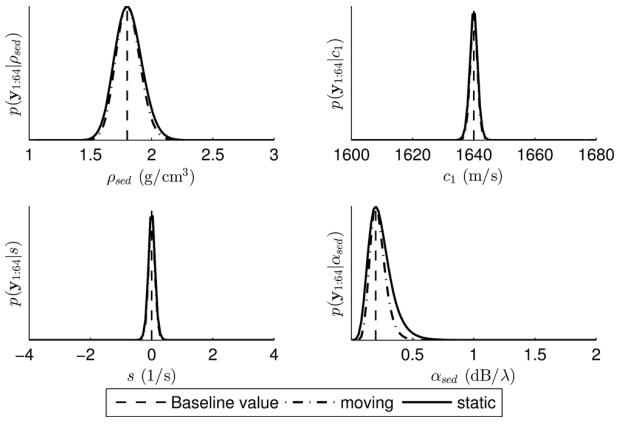

FIG. 8. Likelihood function $p(\mathbf{y}_{1:64}|m_i)$ while fixing the remaining model parameters to the baseline values (see Table III) for moving/static source-receiver configurations.

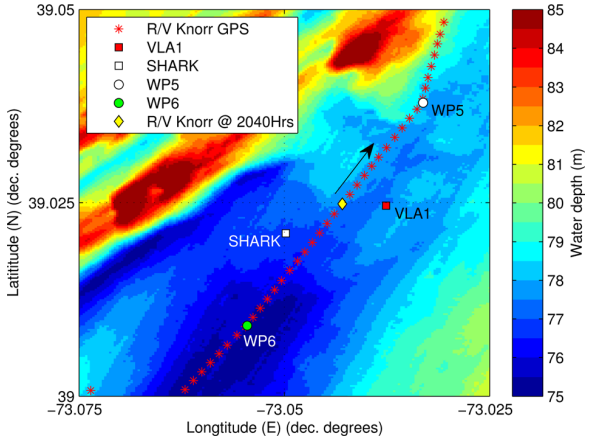

FIG. 9. (Color online) SW06 experiment site, bathymetry, source, and receiver positions on JD238 (26 Aug 2006) 2000–2059 UTC.

measured SSP is known to be range dependent and is not a good substitute for an averaged range independent SSP. In addition, due to the lack of conductivity, temperature and depth (CTD) measurements during this period and location, sound speed profile inversion was included using empirical orthogonal functions[42–44] (EOFs) based on SSPs derived from thermistors along the SHARK array (see Fig. 9).[1]

A. Data preprocessing and inversion results

Pre-processing of the single receiver data for all L pulses includes LFM pulse matched filtering for coarse synchronization (Fig. 11). The data then are sliced according to the synchronization and FFT'd to obtain the measured field $\mathbf{y}_l$ for each pulse in the frequency domain. The matched filter output is not used in the inversion itself. Finally, the frequency domain data are phase-adjusted according to the synchronization times such that coherent combination will follow Eq. (5). This makes the timing reference the same for all frequency domain data. For computational reasons, the frequency sampling interval is 5 Hz from 100 to 700 Hz. As explained in Ref. 1 and in Sec. II

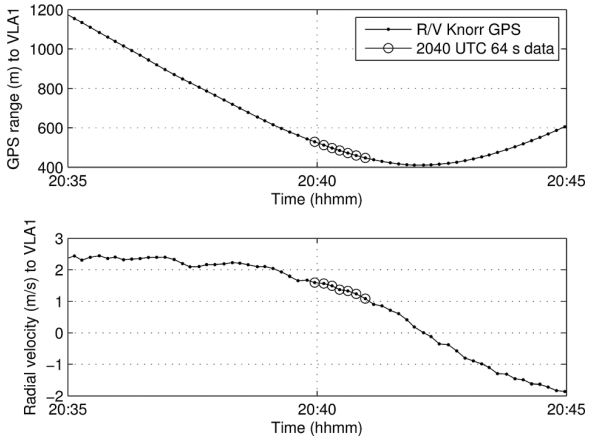

FIG. 10. R/V Knorr range and radial velocity to VLA1. Highlighted is the period of time corresponding to the 64 s data analyzed.

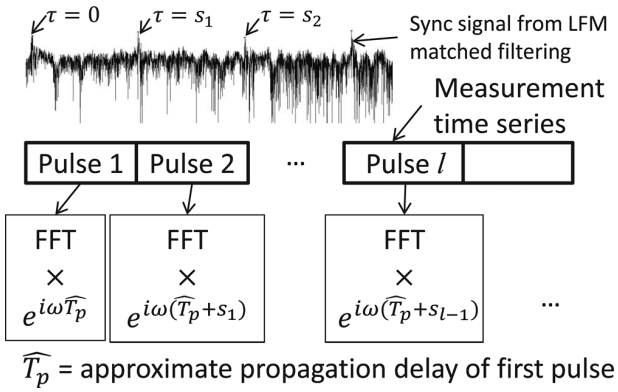

FIG. 11. LFM pulse matched filtering for coarse synchronization.

A, the advantage of the waveguide Doppler model is that the forward model is computed on the receiver frequencies. To construct the replica field for a receiver frequency, the forward model has to trace backward to multiple source frequencies due to mode-dependent Doppler shifts. This is done analytically using the backward frequency mapping in Eq. (7). The forward and backward mapping relationships between the source, propagation and receiver frequencies are provided in Table IV.[1]

The lower and upper bounds for the model parameters priors were set for the forward model depicted in Fig. 1 based on the background information at the experiment site,[1,19,43,44,47,48] see Table V. Importance samples are drawn from Gaussian mixtures, and uniform priors are assumed. The 18-parameter recursive Bayesian inversion was done for $L = [1, \ldots, 64]$ using an initial 240 000 importance samples $(L = 1)$ that eventually grows to 840 000 importance samples $(L = 64)$. Note that a high number of importance samples is necessary for good PPD estimation.[4] On the other hand, MAP estimates require considerably fewer importance samples than required for PPD estimation.[41]

Table V tabulates the inversion MAP results using waveguide Doppler without and with acceleration modeled for the 64 LFM pulses. For the inversion results using the acceleration model, the estimated sediment thickness, velocity, and density are consistent with other published results[1,19,43,44,47,48] at the VLA1 site. For example, these inversion results range from 1600 to 1670 m/s for the top sediment velocity and 20 to 25 m for the sediment thickness. In addition, the geometric parameters (r_0, z_s, z_r, v_{s1}, a_s, and z_w) results also agree very well with the measured or best known values. However, the gradient of the sediment velocity remains inconclusive.[19] There have been negative, zero, and positive gradient sediment profile inversion results obtained by different investigators. The negative gradient sediment profile results here are similar to the results in Ref. 44.

TABLE IV. Mapping relationships for the source, propagation and receiver frequencies.

Source	Propagation	Receiver
$\omega_s^{(k_{nl})} = \omega_r - k_{nl}(v_{sl} - v_{rl})$	$\omega = \omega_r + k_{nl} v_{rl}$	ω_r
ω_s	$\omega = \omega_s + k_{nl} v_{sl}$	$\omega_r^{(k_{nl})} = \omega_s + k_{nl}(v_{sl} - v_{rl})$

The posterior densities of the model parameters are illustrated in Figs. 12–14, where only the 1-D (plots along the diagonal) and 2-D (plots above the diagonal) marginal PPDs are shown. Only the most relevant 11 or 12 of 18 parameters are given in Figs. 12–14. The three EOF coefficients PPDs are difficult to interpret in terms of the water column SSP uncertainties. Therefore the uncertainties or PPDs of the water column SSP, using Bayesian inference [Eq. (23)], are plotted from the PPD statistics of the EOF coefficients.

Comparing Figs. 12 and 14, the reduction in uncertainties between $L = 1$ and $L = 64$ is remarkably good across all parameters. Uncertainty reduction in the water column SSP also is observed (see Figs. 12 and 14). The largest uncertainty in the water column SSP is between 35 and 45 m depth. This compares well to the SHARK SSP measurements between 1830 and 2229 UTC where the largest sound speed variation is around 40 m depth (see Fig. 14). Because the SSPs are known to be range dependent in SW06, the SHARK SSP measured at 2040 UTC was not a good substitute for an averaged range independent SSP. The EOFs have enabled the inversion to optimize for the best average SSP and the SSP inverted here is consistent with the SSP inversion results from Ref. 1.

In contrast, the MAP results in Table V for $L = 64$ without using the acceleration model yield more biased geometric and geophysical (r_0, z_s, z_r, z_w, and ρ_{sed}) results when compared to measured or best known values. The biased geometric results are an indication that this inversion is not reliable. For example, the source range r_0 is 50 m short and the water, source and receiver depth, are, respectively, 4.8, 1.2, and 3.6 m too shallow. These differences cannot be explained by the effective parameter calculations for a mildly range dependent environment.[50] This further is

TABLE V. SW06 data inversion parameters prior bounds and MAP results for $L = 64$.

Model parameters	Prior Lower limit	Prior Upper limit	Without a_s option	With a_s option
Src range at $t = 0$, r_0 (m)	520	630	550	594
Src depth, z_s (m)	27	32	28.8	29.7
Rcv depth, z_r (m)	39	46	41.0	42.6
Timing error, ξ (ms)	−50	50	9	−20
Src rad. vel., v_{s1} (m/s)	1.5	2.0	1.84	1.94
Src rad. accel., a_s (mm/s^2)	−7	−5	N/A	−6
EOF1 coef.	−50	50	22.5	42.3
EOF2 coef.	−20	20	6.6	14.0
EOF3 coef.	−10	10	0.9	5.2
Sed. thickness, h_{sed} (m)	10	30	20.5	21.5
Sed. dens., ρ_{sed} (g/cm^3)	1	3	2.5	2.1
Sed. attn., α_{sed} (dB/λ)	0.001	1	0.2	0.3
Sed. top. vel., c_1 (m/s)	1550	1700	1644	1655
Sed. vel. slope, s (1/s)	−10	10	−3.3	−4.3
Bot. vel., c_b (m/s)	1600	2200	1967	1993
Water depth, z_w (m)	74	81	74.2	76.9
Src level, α	0.1	0.8	0.2	0.5
Noise level, γ	0.5	1.9	1.5	1.1

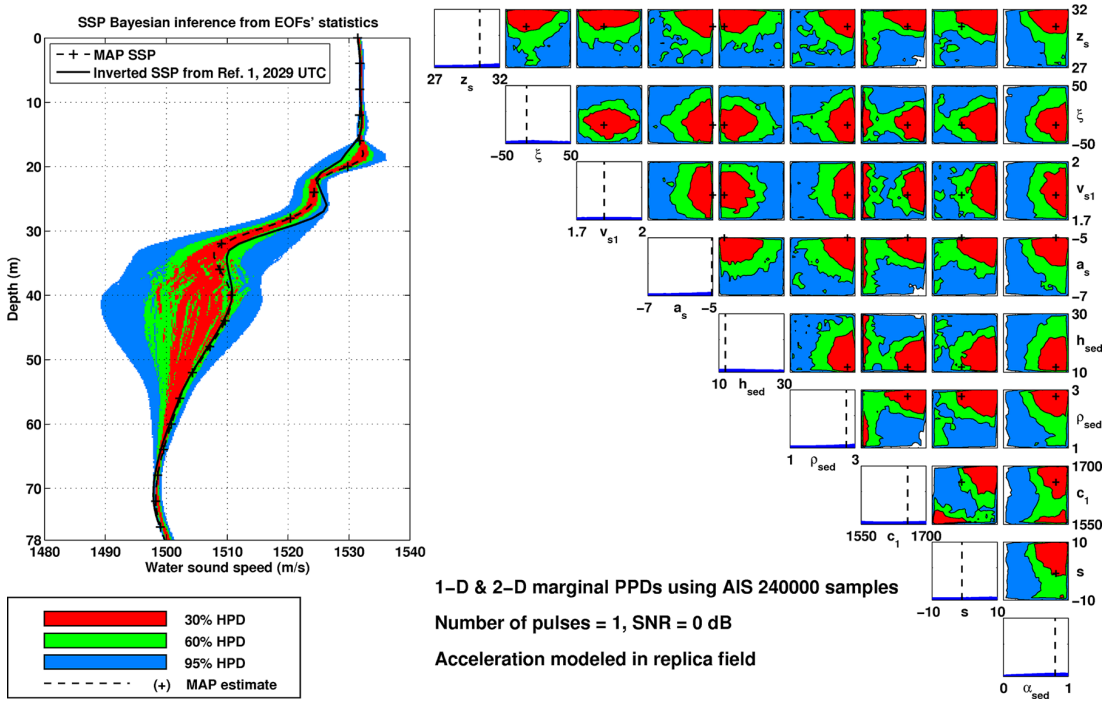

FIG. 12. (Color online) SW06 data recursive Bayesian inversion results using the waveguide Doppler model with acceleration modeled in the replica for $L = 1$.

supported by the parameter estimation uncertainties or the 95% HPD region results when not using acceleration which are about 100% more than the results when using the acceleration model (compare Figs. 13 and 14). The inverted water column velocity profile also is different than the results when using the acceleration model. Thus the quality of the inversion results without modeling acceleration is lower than that with acceleration modeled.

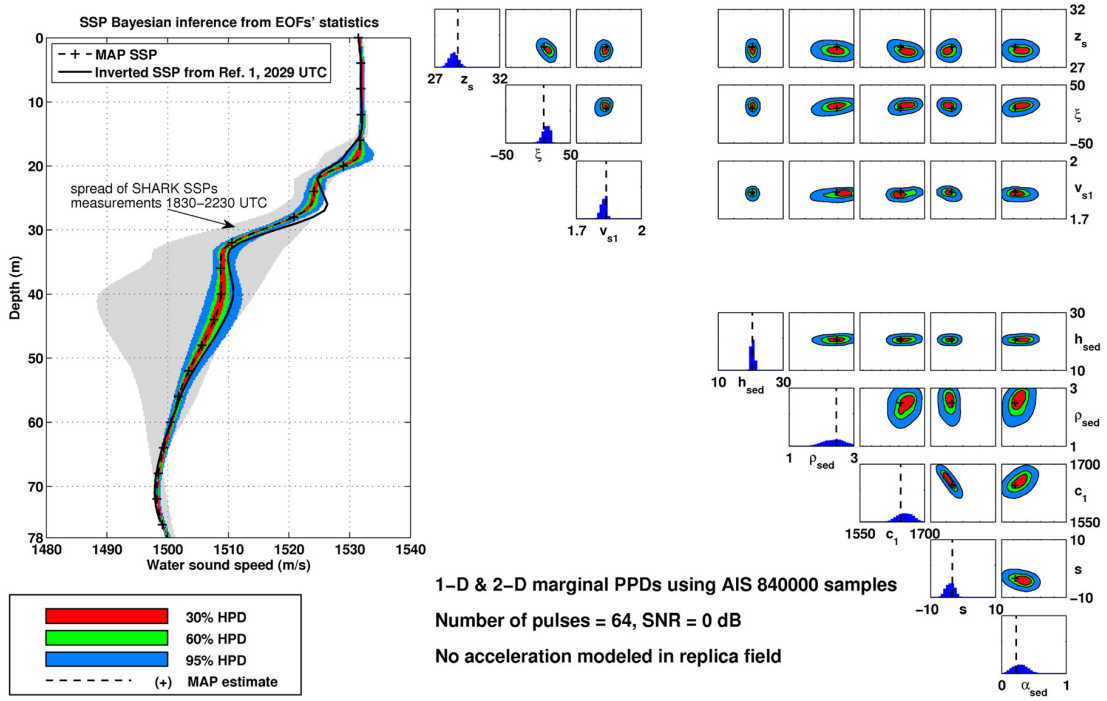

FIG. 13. (Color online) SW06 data recursive Bayesian inversion results using the waveguide Doppler model with no acceleration modeled in the replica for $L = 64$.

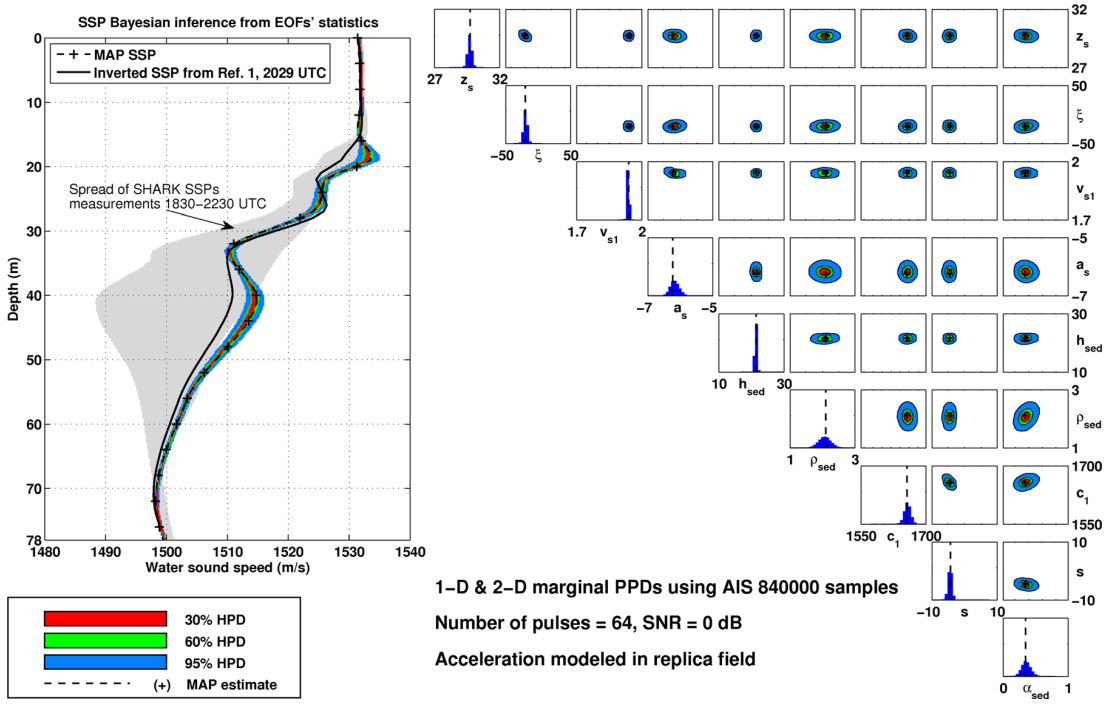

FIG. 14. (Color online) SW06 data recursive Bayesian inversion results using the waveguide Doppler model with acceleration modeled in the replica for $L = 64$.

V. CONCLUSIONS

A broadband, frequency coherent matched-field inversion procedure for a moving source and receiver at low SNR using a recursive Bayesian pulse-by-pulse approach has been developed. This enabled a time-evolving uncertainty analysis of the model parameters and an approximation for a horizontally accelerating source and receiver. Through simulation and data analysis from the Shallow Water 2006 experiment, it was demonstrated that: (1) Via online uncertainty analysis, parameter uncertainty reduces with an increasing number of pulses and (2) when source/receiver acceleration exists, modeling acceleration in the inversion can reduce further parameter estimation biases and uncertainties.

ACKNOWLEDGMENTS

This work was supported by the Office of Naval Research Grant No. N00014-11-0320 and the DSO National Laboratories of Singapore.

[1]B. A. Tan, P. Gerstoft, C. Yardim, and W. S. Hodgkiss, "Broadband synthetic aperture geoacoustic inversion," J. Acoust. Soc. Am. **134**, 312–322 (2013).
[2]H. Schmidt and W. A. Kuperman, "Spectral and modal representations of the Doppler-shifted field in ocean waveguides," J. Acoust. Soc. Am. **96**, 386–395 (1994).
[3]F. B. Jensen, W. A. Kuperman, M. B. Porter, and H. Schmidt, *Computational Ocean Acoustic, Modern Acoustics and Signal Processing*, 2nd ed. (Springer, New York, 2011), pp. 623–629.
[4]C. Yardim, P. Gerstoft, and W. S. Hodgkiss, "Statistical maritime radar duct estimation using hybrid genetic algorithm Markov Chain Monte Carlo method," Radio Sci. **42**, RS3014, doi: 10.1029/2006RS003561 (2007).
[5]C.-F. Huang, P. Gerstoft, and W. S. Hodgkiss, "Validation of statistical estimation of transmission loss in the presence of geoacoustic inversion uncertainty," J. Acoust. Soc. Am. **120**, 1932–1941 (2006).
[6]R. Duda, P. Hart, and D. Stork, *Pattern Classification*, 2nd ed. (Wiley, New York, 2001), pp. 97–98, 531–534.
[7]J. Bonnel, C. Gervaise, B. Nicolas, and J. I. Mars, "Single-receiver geoacoustic inversion using modal reversal," J. Acoust. Soc. Am. **131**, 119–128 (2012).
[8]J. Bonnel and N. R. Chapman, "Geoacoustic inversion in a dispersive waveguide using warping operators," J. Acoust. Soc. Am. **130**, EL101–EL107 (2011).
[9]J. Bonnel, B. Nicolas, J. I. Mars, and S. C. Walker, "Estimation of modal group velocities with a single receiver for geoacoustic inversion in shallow water," J. Acoust. Soc. Am. **128**, 719–727 (2010).
[10]C. Gervaise, B. G. Kinda, J. Bonnel, Y. Stephan, and S. Vallez, "Passive geoacoustic inversion with a single hydrophone using broadband ship noise," J. Acoust. Soc. Am. **131**, 1999–2010 (2012).
[11]N. F. Josso, C. Ioana, J. I. Mars, and C. Gervaise, "Source motion detection, estimation, and compensation for underwater acoustics inversion by wideband ambiguity lag-Doppler filtering," J. Acoust. Soc. Am. **128**, 3416–3425 (2010).
[12]N. F. Josso, C. Ioana, J. I. Mars, C. Gervaise, and Y. Stephan, "On the consideration of motion effects in the computation of impulse response for underwater acoustics inversion," J. Acoust. Soc. Am. **126**, 1739–1751 (2009).
[13]J. C. Le Gac, M. Asch, Y. Stephan, and X. Demoulin, "Geoacoustic inversion of broad-band acoustic data in shallow water on a single hydrophone," IEEE J. Ocean. Eng. **28**, 479–493 (2003).
[14]S. M. Jesus, M. B. Porter, Y. Stephan, X. Demoulin, O. C. Rodriguez, and E. M. M. F. Coelho, "Single hydrophone source localization," IEEE J. Ocean. Eng. **25**, 337–346 (2000).
[15]P. Hursky, M. B. Porter, M. Siderius, and V. K. McDonald, "High-frequency (8–16 kHz) model-based source localization," J. Acoust. Soc. Am. **115**, 3021–3032 (2004).
[16]J. P. Hermand, "Broad-band geoacoustic inversion in shallow water from waveguide impulse response measurements on a single hydrophone: Theory and experimental results," IEEE J. Ocean. Eng. **24**, 41–66 (1999).
[17]M. Siderius, P. Gerstoft, and P. L. Nielsen, "Broadband geo-acoustic inversion from sparse data using genetic algorithms," J. Comp. Acoust. **6**, 117–134 (1998).
[18]G. V. Frisk, J. F. Lynch, and S. D. Rajan, "Determination of compressional wave speed profiles using modal inverse techniques in a range-dependent environment in Nantucket sound," J. Acoust. Soc. Am. **86**, 1928–1939 (1989).

[19]J. Bonnel, S. E. Dosso, and N. Ross Chapman, "Bayesian geoacoustic inversion of single hydrophone light bulb data using warping dispersion analysis," J. Acoust. Soc. Am. **134**, 120–130 (2013).
[20]D. P. Massa and J. I. Arvelo, "A wideband moving coil electrodynamic transducer system for autonomous underwater vehicle-based geoacoustic inversion," J. Acoust. Soc. Am. **132**, 1920 (2012).
[21]P. L. Nielsen, C. W. Holland, and L. Troiano, "Geoacoustic characterization and bottom scattering measurements using an autonomous underwater vehicle," Technical Report CMRE-FR-2012-005, North Atlantic Treaty Organization Centre for Maritime Research and Experimentation, La Spezia, Italy (2012).
[22]P. L. Nielsen, M. Siderius, J. Miller, S. Crocker, and J. Giard, "Seabed characterization using ambient noise and compact arrays on an autonomous underwater vehicle," in *Proceedings of Meetings on Acoustics* Montreal, Quebec, Canada (2013), Vol. 19, p. 070 030.
[23]C. W. Holland, P. L. Nielsen, J. Dettmer, and S. Dosso, "Resolving mesoscale seabed variability using reflection measurements from an autonomous underwater vehicle," J. Acoust. Soc. Am. **131**, 1066–1078 (2012).
[24]N. P. Chotiros and V. Pallayil, "Seabed characterization using acoustic communication signals on an autonomous underwater vehicle with a thin-line towed array," IEEE J. Ocean. Eng. **38**, 410–418 (2013).
[25]K. E. Hawker, "A normal mode theory of acoustic Doppler effects in the oceanic waveguide," J. Acoust. Soc. Am. **65**, 675–681 (1979).
[26]H. C. Song and A. B. Baggeroer, "The resolution of modal Doppler shifts in a dispersive oceanic waveguide," J. Acoust. Soc. Am. **88**, 268–282 (1990).
[27]P. B. Weichman, "Doppler effects in heterogeneous media with applications to ocean acoustic modeling," Phys. Rev. E **72**, 066602 (2005).
[28]M. H. Brill, "Nonreciprocity of acoustic Doppler effect: Proof and physical mechanism," Phys. Essays **24**, 570–573 (2011).
[29]S. C. Walker, P. Roux, and W. A. Kuperman, "Modal Doppler theory of an arbitrarily accelerating continuous-wave source applied to mode extraction in the oceanic waveguide," J. Acoust. Soc. Am. **122**, 1426–1439 (2007).
[30]A. Papoulis and S. Pillai, *Probability, Random Variables, and Stochastic Processes*, 4th ed. (McGraw-Hill, New York, 2002), pp. 515, 519.
[31]C. Yardim, P. Gerstoft, and W. S. Hodgkiss, "Geoacoustic and source tracking using particle filtering: Experimental results," J. Acoust. Soc. Am. **128**, 75–87 (2010).
[32]C. Yardim, P. Gerstoft, and W. S. Hodgkiss, "Sequential geoacoustic inversion at the continental shelfbreak," J. Acoust. Soc. Am. **131**, 1722–1732 (2012).
[33]A. Doucet, S. Godsill, and C. Andrieu, "On sequential Monte Carlo sampling methods for Bayesian filtering," Stat. Comput. **10**, 197–208 (2000).
[34]B. Ristic, S. Arulampalam, and N. Gordon, *Beyond the Kalman Filter: Particle Filters for Tracking Applications* (Artech House, Boston, 2004), pp. 35–39.
[35]D. Lee and N. Chia, "A particle algorithm for sequential Bayesian parameter estimation and model selection," IEEE Trans. Sig. Proc. **50**, 326–336 (2002).
[36]C. Yardim, Z. H. Michalopoulou, and P. Gerstoft, "An overview of sequential Bayesian filtering in ocean acoustics," IEEE J. Ocean. Eng. **36**, 71–89 (2011).
[37]C.-F. Huang, P. Gerstoft, and W. S. Hodgkiss, "Uncertainty analysis in matched-field geoacoustic inversions," J. Acoust. Soc. Am. **119**, 197–207 (2006).
[38]J. Geweke, "Bayesian inference in econometric models using Monte Carlo integration," Econometrica1 **57**, 1317–1339 (1989).
[39]J. J. K. Ruanaidh and W. J. Fitzgerald, *Numerical Bayesian Methods Applied to Signal Processing* (Springer, New York, 1996), pp. 31, 51–61.
[40]D. J. C. MacKay, *Information Theory, Inference and Learning Algorithms* (Cambridge University Press, Cambridge, UK, 2003), pp. 357–364.
[41]P. Gerstoft and C. F. Mecklenbrauker, "Ocean acoustic inversion with estimation of a posteriori probability distributions," J. Acoust. Soc. Am. **104**, 808–819 (1998).
[42]P. Gerstoft and D. F. Gingras, "Parameter estimation using multifrequency range-dependent acoustic data in shallow water," J. Acoust. Soc. Am. **99**, 2839–2850 (1996).
[43]C.-F. Huang, P. Gerstoft, and W. S. Hodgkiss, "Effect of ocean sound speed uncertainty on matched-field geoacoustic inversion," J. Acoust. Soc. Am. **123**, EL162–EL168 (2008).
[44]Y.-M. Jiang and N. R. Chapman, "Bayesian geoacoustic inversion in a dynamic shallow water environment," J. Acoust. Soc. Am. **123**, EL155–EL161 (2008).
[45]A. B. Owen, "Monte Carlo theory, methods and examples," (2013), http://statweb.stanford.edu/ owen/mc/, Chaps. 9 and 10 (Last viewed 3/10/2014).
[46]O. Cappé, R. Douc, A. Guillin, J.-M. Marin, and C. P. Robert, "Adaptive importance sampling in general mixture classes," Stat. Comput. **18**, 447–459 (2008).
[47]J. W. Choi, P. H. Dahl, and J. A. Goff, "Observations of the R reflector and sediment interface reflection at the shallow water '06 central site," J. Acoust. Soc. Am. **124**, EL128–EL134 (2008).
[48]C. Park, W. Seong, P. Gerstoft, and W. S. Hodgkiss, "Geoacoustic inversion using backpropagation," IEEE J Ocean. Eng. **35**, 722–731 (2010).
[49]M. B. Porter, "The KRAKEN normal mode program," SACLANTCEN Memo. SM-245, SACLANT Undersea Research Centre, La Spezia, Italy (1991), Chap. 2.
[50]C. Harrison and M. Siderius, "Effective parameters for matched field geoacoustic inversion in range-dependent environments," IEEE J. Ocean. Eng. **28**, 432–445 (2003).